On the closed-form evaluation of the PO integral using the Radon transform interpretation for linear triangles

Aslihan AKTEPE[*]💿**, Hüseyin Arda ÜLKÜ**💿
Department of Electronics Engineering, Gebze Technical University, Kocaeli, Turkey

Abstract: This letter presents the complete mathematical formulation for the closed-form evaluation of the time domain physical optics (PO) integral on linear triangular patches using Radon transform (RT) interpretation. The incident field is assumed to be an impulsively excited plane wave and scattered fields are observed at far-zone. The PO integral is evaluated in closed-form as the intersection of the triangle and the plane formed by the incident and observation directions. In addition, a formula is suggested for the special case, which occurs if there is no intersection of the plane and all scatterer. Accuracy of the closed-form expressions is demonstrated via numerical examples.

Key words: Closed-form evaluation, physical optics approximation, Radon transform interpretation, time domain analysis

1. Introduction

Accurate and fast evaluation of the physical optics (PO) integral is very important on the application of PO approximation to the analysis of electrically large scatterers [1–7]. In the literature, it is possible to find plenty of works that searched for an approximate or exact expression to the PO integral both in the time and frequency domains for different geometric formations [1–9]. An elegant way to evaluate the closed-form expression of the PO integral for linear triangular patches in time domain (and also Fourier transformed to frequency domain) is presented in [2] using the Radon transform (RT) interpretation. In [2], the PO integral over a linear triangular surface is reduced to a line integral over the intersection of the linear triangle and the plane formed by the propagation direction of the incident plane wave and the observation direction, called $\mathbf{k}_r$-plane, then it is concluded that the closed-form expression to the line integral should be a triangle function since the domain of the PO integral is a linear triangle. This approach is also extended to non-uniform rational basis spline (NURBS) surfaces [8], quadratic triangular patches [9], different source and observation configurations [3, 4], even applied to time domain integral equations [10]. However, the closed-form expression presented in [2] can be obtained mathematically following the steps applied in [9] for exact evaluation of the PO integral for quadratic triangles. In addition, for a time domain simulation, it is possible to encounter with a case such that all scatterer can be completely fit into two consecutive time samples, resulting in no intersection. This case is not the specular reflection case (i.e., the special case that the $\mathbf{k}_r$-plane is parallel to the triangular patch) and strongly depends on the choice of the time step size, the incidence, and observation directions. This case is called under-sampled reflection (USR) case in this letter. Note that USR case has not been encountered in [2] since all examples in [2] are produced in frequency domain even the formulation is partially in time domain.

[*]Correspondence: aaktepe@gtu.edu.tr

The contributions of this letter are in threefold: (i) the mathematically complete formulation of the closed-form evaluation of the PO integral for a linear triangular patch in time domain step by step without any interpretation is presented. The incident field is assumed to be an impulsively excited plane wave and far scattered fields are observed as in [2]. Note that the formulation presented in this letter is based on the exact evaluation scheme in [9] and its simplification to linear triangles, which yields a less complex formulation and closed-form evaluation. (ii) For the USR case, a formula, which has a rectangular shape in time, is proposed. Specifically, the temporal integral of the proposed formula yields the area of the linear triangle, which is also same as the temporal integral of the PO integral. The accuracy of the proposed formula for the USR case is analyzed via numerical examples. (iii) In addition, it is shown that the accuracy of the scattered field obtained using the time domain PO approximation strongly depends on the norm of $\mathbf{k}_r$, besides the time step size. Note that this observation might be crucial to maintain the accuracy at the same level for all incident/observation directions.

The rest of the letter is organized as follows: Section 2 presents the formulation for closed-form evaluation of the PO integral in time domain and the suggested formula for USR case. In Section 3, numerical examples are presented, and in Section 4 conclusions are drawn.

2. Formulation

Let S denote the surface of a perfect electrically conducting (PEC) scatterer that resides in an infinite homogeneous background medium with permittivity ε_0 and permeability μ_0. The electric field component of the impulsively excited incident plane wave $\mathbf{E}^{\text{inc}}(\mathbf{r}, t) = \hat{\mathbf{p}}\delta(t - \hat{\mathbf{k}}_i \cdot \mathbf{r}/c)$, where $\hat{\mathbf{k}}_i$ and $\hat{\mathbf{p}}$ are the propagation direction and polarization of the incident wave, respectively, $\delta(\cdot)$ denotes the Dirac delta function, and $c = 1/\sqrt{\varepsilon_0 \mu_0}$ is the speed of light. In the PO approximation, the current density is assumed as $\mathbf{J}(\mathbf{r}, t) = 2\hat{\mathbf{n}}(\mathbf{r}) \times \mathbf{H}^{\text{inc}}(\mathbf{r}, t)$; $\mathbf{r} \in S_{\text{lit}}$, and $\mathbf{J}(\mathbf{r}, t) = 0$; $\mathbf{r} \in S_{\text{sha}}$, where $\hat{\mathbf{n}}(\mathbf{r})$ denotes the outward pointing unit normal vector of S, $\mathbf{H}^{\text{inc}}(\mathbf{r}, t)$ denotes the incident magnetic field intensity, S_{lit} and S_{sha} denote the illuminated and shadowed parts of S. Assuming that S_{lit} is discretized with linear triangular patches, $S_{\text{lit}} \simeq \bigcup_{n=1}^{N} S_n$, the scattered electric field intensity at far-zone can be determined as

$$\mathbf{E}^{\text{sca}}(\mathbf{r}, t) = -\frac{1}{2\pi c}\frac{\partial_t \delta(t - r/c)}{r} * \left[\hat{\mathbf{k}}_s \times \hat{\mathbf{k}}_s \times (\hat{\mathbf{k}}_i \times \hat{\mathbf{p}}) \times \sum_{n=1}^{N} \hat{\mathbf{n}}_n h_n(t) \right], \quad (1)$$

where $\mathbf{r} = r\hat{\mathbf{k}}_s$ and $\hat{\mathbf{k}}_s$ is the observation direction, ∂_t and "$*$" denote the time derivative and convolution, respectively, $\hat{\mathbf{n}}_n = \hat{\mathbf{n}}(\mathbf{r})$; $\mathbf{r} \in S_n$, denotes the unit normal vector of the nth triangular patch, and $h_n(t)$ denotes the PO integral:

$$h_n(t) = \int_{S_n} \delta\left(t - 2c^{-1}\mathbf{k}_r \cdot \mathbf{r}'\right) d\mathbf{r}'. \quad (2)$$

Here $\mathbf{k}_r = (\hat{\mathbf{k}}_i - \hat{\mathbf{k}}_s)/2$. Note that in (2) the argument of the Dirac delta function defines a plane with a time dependent location $t = 2c^{-1}\mathbf{k}_r \cdot \mathbf{r}'$, called $\mathbf{k}_r$-plane. Considering the infinite time integral of $h_n(t)$ yields the area of the triangular surface S_n, time samples of $h_n(t)$ are the intersection of the $\mathbf{k}_r$-plane and the triangular surface S_n. Since S_n is a linear triangular surface, the result of the integral should be a triangle function [2] (see Figure 1 in [2]). Next the closed-form evaluation of $h_n(t)$ is shown.

2.1. Evaluation of $h_n(t)$

A linear triangular patch is defined by three nodes $\mathbf{r}_1$, $\mathbf{r}_2$, $\mathbf{r}_3$, and assume that these nodes are ordered in intersection time of the node and the $\mathbf{k}_r$-plane as $t_3 > t_2 > t_1$, where $t_i = 2c^{-1}\mathbf{k}_r \cdot \mathbf{r}_i$, $i = 1, 2, 3$, as shown in Figure 1 in [2]. Any point on S_n can be pointed using barycentric coordinates of S_n, i.e. $\mathbf{r}' = (\mathbf{r}_2 - \mathbf{r}_1)\alpha + (\mathbf{r}_3 - \mathbf{r}_1)\beta + \mathbf{r}_1$, where (α, β) denote the barycentric coordinates as shown in Figure 1. The coordinate system can be rotated as $(x, y, z) \rightarrow (x_p, y_p, z_p)$ such that $\mathbf{k}_r \parallel \hat{\mathbf{x}}_p$. As a result intersection time can be given as $t_i = 2c^{-1} |\mathbf{k}_r| x_{p,i}$, $i = 1, 2, 3$, and using the Dirac delta function's property $\delta(ax) = |a|^{-1}\delta(x)$ [11], $h_n(t)$ can be written as

$$h_n(t) = \frac{c}{2|\mathbf{k}_r|} \int_{S_n} \delta\left(\frac{ct}{2|\mathbf{k}_r|} - x'_{p,i}\right) d\mathbf{r}_p. \tag{3}$$

The argument of the Dirac delta function in (3) determines the location of the $\mathbf{k}_r$-plane:

$$0 = \frac{ct}{2|\mathbf{k}_r|} - x'_{p,i} = \frac{ct}{2|\mathbf{k}_r|} - [(x_{p,2} - x_{p,1})\alpha + (x_{p,3} - x_{p,1})\beta + x_{p,1}]. \tag{4}$$

A coordinate transformation as shown in Figure 1 is applied to (3) and (4),
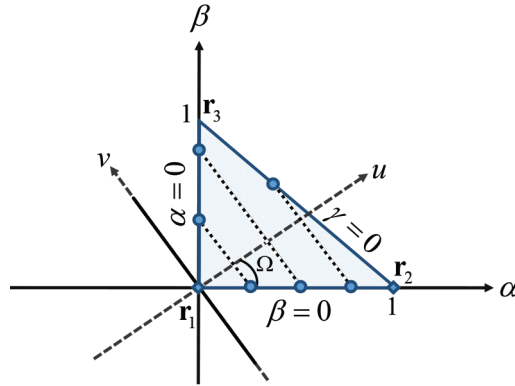
Figure 1. Intersection of the $\mathbf{k}_r$-plane and S_n in the barycentric coordinates.

$$\alpha = u \cos\Omega - v \sin\Omega \tag{5}$$

$$\beta = u \sin\Omega + v \cos\Omega,$$

where $\Omega = \tan^{-1}[(x_{p,3} - x_{p,1})/(x_{p,2} - x_{p,1})]$. Note that since $t_3 > t_2 > t_1$ (also $x_{p,3} > x_{p,2} > x_{p,1}$), $\Omega \in [0, \pi/2)$. Substituting (5) into (4) yields

$$u = \frac{1}{\tau}\left[\frac{ct}{2|\mathbf{k}_r|} - x_{p,1}\right], \tag{6}$$

where $\tau = \sqrt{(x_{p,2} - x_{p,1})^2 + (x_{p,3} - x_{p,1})^2}$. Applying the coordinate transformation in (5) to the PO integral (3) yields

$$h_n(t) = \frac{ctA_n}{\tau|\mathbf{k}_r|} \int_u \delta\left(u - \frac{ct}{2|\mathbf{k}_r|\tau} + \frac{x_{p,1}}{\tau}\right) \int_{v(u)} dv\, du. \tag{7}$$

Here, $A_n = 0.5 \left| (\mathbf{r}_3 - \mathbf{r}_1) \times (\mathbf{r}_2 - \mathbf{r}_1) \right|$ denotes the area of the triangle, $2A_n$ is the Jacobean of the transformation. The integral w.r.t. u in (7) can be evaluated analytically using the Dirac delta function's property $\int f(x)\delta(x - x_0)dx = f(x_0)$ [11] as

$$h_n(t) = \frac{ctA_n}{\tau \left| \mathbf{k}_\mathrm{r} \right|} \int_{v(u)} dv \Bigg|_{u = \frac{ct}{2|\mathbf{k}_\mathrm{r}|\tau} - \frac{x_{p,1}}{\tau}}. \tag{8}$$

Note that in (u,v), $\mathbf{k}_\mathrm{r} \parallel v$ and the integral in (8) represents the line that is formed as a result of the intersection of the $\mathbf{k}_\mathrm{r}$-plane and S_n. In addition, since $t_3 > t_2 > t_1$; the $\mathbf{k}_\mathrm{r}$-plane first intersects with $\mathbf{r}_1$ (where $\alpha = 0$ and $\beta = 0$), then intersects with $\mathbf{r}_2$ (where $\alpha = 1$ and $\beta = 0$), and lastly intersects with $\mathbf{r}_3$ (where $\alpha = 0$ and $\beta = 1$). This order determines the limits of the integral in (8). Hence the integral in (8) should be evaluated for two regions: for $t_2 > t > t_1$, the lower and upper limits are on $\beta = 0$ and $\alpha = 0$ lines, respectively. For $t_3 > t > t_2$ they are on $\alpha = 0$ and $\gamma = 1 - \alpha - \beta = 0$ lines, respectively. For a given u, intersection of the v axis with $\beta = 0$, $\alpha = 0$, and $\gamma = 1 - \alpha - \beta = 0$ lines can be found using the inverse transformation of (5) as

$$v_\beta(u) = \frac{-u \sin \Omega}{\cos \Omega} = \frac{-u(x_{p,3} - x_{p,1})}{(x_{p,2} - x_{p,1})}, \tag{9}$$

$$v_\alpha(u) = \frac{u \cos \Omega}{\sin \Omega} = \frac{u(x_{p,2} - x_{p,1})}{(x_{p,3} - x_{p,1})}, \tag{10}$$

$$v_\gamma(u) = \frac{1 - u[\cos \Omega + \sin \Omega]}{\cos \Omega - \sin \Omega} \tag{11}$$

$$= \frac{\tau - u[x_{p,2} + x_{p,3} - 2x_{p,1}]}{x_{p,2} - x_{p,3}},$$

respectively. As a result, the closed-form expression of $h_n(t)$ in (8) can be determined for $t_2 > t > t_1$ as

$$h_n(t) = \frac{ctA_n}{\left| \mathbf{k}_\mathrm{r} \right| \tau} [v_\alpha(u) - v_\beta(u)]_{u = \frac{ct}{2|\mathbf{k}_\mathrm{r}|\tau} - \frac{x_{p,1}}{\tau}} \tag{12}$$

$$= \frac{ctA_n}{\left| \mathbf{k}_\mathrm{r} \right| \tau^2} \left[\frac{ct}{2 \left| \mathbf{k}_\mathrm{r} \right|} - x_{p,1} \right] \left[\frac{\tau^2}{(x_{p,3} - x_{p,1})(x_{p,2} - x_{p,1})} \right]$$

$$= \frac{ctA_n}{\left| \mathbf{k}_\mathrm{r} \right|} \frac{\frac{ct}{2|\mathbf{k}_\mathrm{r}|} - x_{p,1}}{(x_{p,3} - x_{p,1})(x_{p,2} - x_{p,1})}$$

$$= 2A_n \frac{t - t_1}{(t_3 - t_1)(t_2 - t_1)},$$

and for $t_3 > t > t_2$ as

$$h_n(t) = \frac{ctA_n}{\left| \mathbf{k}_\mathrm{r} \right| \tau} [v_\gamma(u) - v_\alpha(u)]_{u = \frac{ct}{2|\mathbf{k}_\mathrm{r}|\tau} - \frac{x_{p,1}}{\tau}} \tag{13}$$

$$= \frac{ctA_n}{\left| \mathbf{k}_\mathrm{r} \right|} \frac{\frac{ct}{2|\mathbf{k}_\mathrm{r}|} - x_{p,3}}{(x_{p,3} - x_{p,1})(x_{p,2} - x_{p,3})}$$

$$= 2A_n \frac{t - t_3}{(t_3 - t_1)(t_2 - t_3)}.$$

If $t > t_3$ or $t_1 > t$, then there is no intersection and $h_n(t) = 0$. Consequently, $h_n(t)$ can be given as follows

$$h_n(t) = \begin{cases} \frac{2A_n(t-t_1)}{(t_2-t_1)(t_3-t_1)}, & (t_1 < t < t_2) \\ \frac{2A_n(t-t_3)}{(t_2-t_3)(t_3-t_1)}, & (t_2 < t < t_3) \\ 0, & \text{elsewhere.} \end{cases} \tag{14}$$

As a special case if $t_1 = t_2 = t_3$, i.e. the specular reflection case, where $\hat{\mathbf{n}}_n \parallel \mathbf{k}_r$ and $\mathbf{k}_r \cdot \mathbf{r}'$ is constant all over S_n, (2) can be written as

$$h_n(t) = \int_{S_n} \delta\left(t - 2\mathbf{k}_r \cdot \mathbf{r}_1/c\right) d\mathbf{r}' \tag{15}$$

$$= \delta\left(t - t_1\right) \int_{S_n} d\mathbf{r}'$$

$$= A_n \delta\left(t - t_1\right)$$

With (14) and (15), the closed-form expressions in [2] are obtained.

2.2. Under-sampled reflection (USR) case

For a time domain simulation a time step size Δt should be selected considering the desired higher limit of the frequency band of the simulation, i.e. $f_{\max}$. The intersection of the scatterer and the $\mathbf{k}_r$-plane occurs in a time interval $t \in [t_{\min}, t_{\max}]$, where $t_{\min} = \min\{2c^{-1}\mathbf{k}_r \cdot \mathbf{r}\}$ and $t_{\max} = \max\{2c^{-1}\mathbf{k}_r \cdot \mathbf{r}\}$, $\forall \mathbf{r} \in S$. Note that $t_{\min}$ and $t_{\max}$ depend on the $\mathbf{k}_r$ direction, which is not a unitary vector and also depends on the incidence and observation directions. If the time step size Δt samples the interval $[t_{\min}, t_{\max}]$, i.e. the $\mathbf{k}_r$-plane intersects with the scatterer at any time sample, then the closed-form expressions given in the previous subsection can be used. However if $(m+1)\Delta t > t_{\max} > t_{\min} > m\Delta t$ for an integer m, then samples of the $\mathbf{k}_r$-plane has no intersection with the scatterer. As a result, the scatterer is totally neglected as it does not exist. This case is named as under-sampled reflection (USR) case in this letter.

In order to remedy this problem, a simple formula is suggested considering the PO integral $h_n(t)$ for a triangle patch is in triangle form in time as in (14) and its temporal integral yields the area of the patch, then $h_n(t)$ can be represented by

$$h_n(t) = \begin{cases} \frac{A_n}{t_3-t_1}, & t_3 > t > t_1 \\ 0, & \text{elsewhere,} \end{cases} \tag{16}$$

where the temporal integral of (16) yields A_n and the Fourier transform of (16) is similar to the Fourier transform of (14) for the frequency $f < f_{\max}$, since Δt is large enough [12].

2.3. Computational complexity

The computational complexity and memory requirement of the PO approximation are different than the marching on-in-time (MOT) based time domain integral equation solvers [13, 14], since, in PO approximation, the solution is obtained without solving a matrix equation. The solution with time domain PO approximation requires $O(N_t N_p)$ operations and $O(N_T)$ memory, where N_p is the number of triangles, N_t is the maximum number of time steps that the $\mathbf{k}_r$-plane and a triangle intersects, N_T is the total number of time steps that samples the scatterer in $[t_{\min}, t_{\max}]$, in other words total number of time steps that the $\mathbf{k}_r$-plane and the

scatterer intersects. For the USR case, both the computational complexity and the memory requirement are $O(N_p)$. N_p, N_t, and N_T depend on Δt, size of the scatterer, norm of $\mathbf{k}_r$, and discretization size. Also it should be emphasized that USR case might be used if the scatterer and the $\mathbf{k}_r$-plane does not intersect, in other words $N_T = N_t = 0$; therefore, it might not be conclusive to compare the computational complexity and memory requirement of the USR case given in Section 2.2 and the time domain PO formulation in Section 2.1.

3. Numerical examples

In all examples presented in this section, a $\hat{\mathbf{p}} = \hat{\mathbf{x}}$ polarized plane wave traveling to $\hat{\mathbf{k}}_i = -\hat{\mathbf{z}}$ direction illuminates the scatterers. The upper frequency limit for simulations $f_{\max} = 2$ GHz (the minimum wave length $\lambda_{\min} = 0.1499$ m) and the time step size is determined by $\Delta t = 1/(2 f_{\max} N_{os})$, where N_{os} denotes the oversampling factor. When $N_{os} = 1$, $\Delta t = 250$ ps is the Nyquist sampling limit for 2 GHz. In all figures, TD denotes the time domain results obtained using (14) and (15), FD denotes the frequency domain results obtained using the formulas given in [2], and USR denotes the case in Section 2.2. Analytical PO solutions for the unit sphere and rectangular plate are given in [15] and [16], respectively. While calculating errors, discrete Fourier transformed TD, FD, and analytical results are calculated at $f = [10$ MHz, 2 GHz$]$ with $\Delta f = 10$ MHz interval, then norm of the relative error in radar cross section (RCS), where all the frequency samples are taken into account.
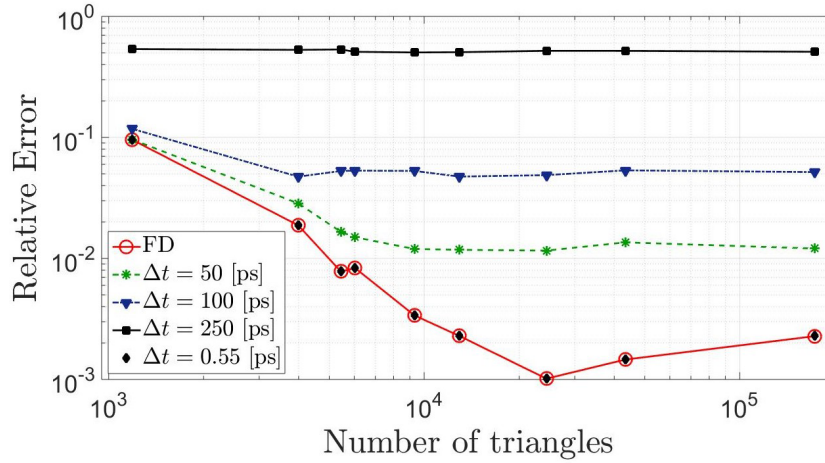
3.1. Unit sphere

First example analyzes the change of the error in the backscattered RCS ($\hat{\mathbf{k}}_s = -\hat{\mathbf{k}}_i$ and $\mathbf{k}_r = \hat{\mathbf{k}}_i$) w.r.t. analytical PO solution as the number of triangles increases. The illuminated part of the unit sphere is discretized with 1188 to 172700 triangles, where the average edge lengths change from $0.77\lambda_{\min}$ to $0.06\lambda_{\min}$. Figure 2 shows the relative errors of FD and TD results for $\Delta t = \{0.55, 50, 100, 250\}$ ps. Note that the relative errors in TD for $\Delta t = \{50, 100, 250\}$ ps saturate and do not decrease as the number of triangles increases, even though time step sizes satisfy the Nyquist sampling criterion. This error is not caused by the discretization since the error of FD results, where time step size has no effect, is lower. The behavior of the error for $\Delta t = \{50, 100, 250\}$ ps is caused because most of the triangles are not taken into account since these triangles do not intersect with the $\mathbf{k}_r$-plane. If the time step size is chosen as small as there is an intersection with all triangles, i.e. TD result for $\Delta t = 0.55$ ps, then the error levels coincide with FD results.
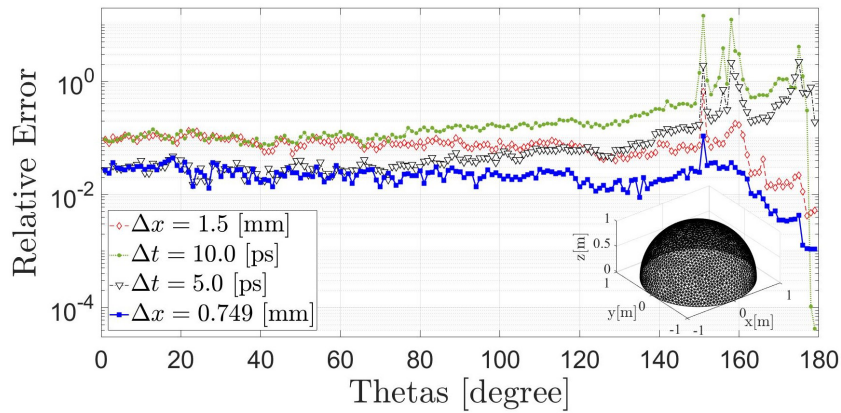
Figure 3 shows the relative error in backscattered RCS obtained by TD w.r.t. FD results to investigate the dependence of the accuracy to $\mathbf{k}_r$ (or $\hat{\mathbf{k}}_s$). $\hat{\mathbf{k}}_s$ is swept between $\theta = [0°, 180°]$ ($\phi = 0°$) and the illuminated part of the unit sphere is discretized with 9307 triangles as shown in Figure 3. Note that $|\mathbf{k}_r|$ changes from 1 to 0 with θ and the spatial step that the $\mathbf{k}_r$-plane takes in a time step changes as $\Delta x = 0.5 c \Delta t |\mathbf{k}_r|^{-1}$. Figure 3 plots the relative error for $\Delta t = \{5.0, 10.0\}$ ps and $\Delta x = \{0.749, 1.5\}$ mm. The former results are obtained by keeping Δt fixed and for the latter ones, Δt is updated to keep Δx fixed, also in these cases no triangles are omitted. It can be seen in Figure 3 that for $\theta < 80°$ the error levels for associated Δt and Δx are coinciding but for $\theta > 80°$, the error for the fixed Δt increases as the error for the fixed Δx remains in the same level.

3.2. Inclined plate

As a second example, backscattered fields ($\hat{\mathbf{k}}_s = -\hat{\mathbf{k}}_i$) of an inclined plate with corners $\mathbf{r}_1 = (-0.5, -0.5, 0)$, $\mathbf{r}_2 = (0.5, -0.5, 0)$, $\mathbf{r}_3 = (0.5, 0.5, 0.1)$, and $\mathbf{r}_4 = (-0.5, 0.5, 0.1)$, modeled with 4 linear triangles (see inset of

Figure 2. Relative error in the backscattered RCS of the unit sphere.

Figure 3. Relative error for $\theta = [0, 180]°$ interval in backscattered RCS.

Figure 4) are analyzed. Figure 4 plots the time domain behavior of $\sum \hat{\mathbf{n}}_n h_n(t)$ for different Δt. It is known that the total PO integral should be in the form of a rectangle function for the plate [8, 16] and, as it can be seen from Figure 4, that the TD results are not satisfactory until $\Delta t = 3.91$ ps ($N_{\mathrm{os}} = 64$). Figure 5 shows the relative error in backscattered RCS obtained by TD results w.r.t. the analytical PO solution as the time step size changes. The relative errors for USR and FD results are also plotted. Note that USR and FD results do not change with Δt. It can be seen from Figure 5 that as the time step size increases, the TD results begin to deteriorate and for $\Delta t > 0.667$ ns, the scatterer fits in two consecutive time steps, TD results become inconclusive, and the error is unitary, since there is no intersection of the $\mathbf{k}_{\mathrm{r}}$-plane and the plate, i.e. $h_n(t) = 0$. For $\Delta t > 0.667$ ns, USR result, which coincides with the FD result very well, can be used in time domain. The error level of TD results coincide with FD result for $\Delta t < 0.0153$ ps ($N_{\mathrm{os}} > 16384$). In addition, this limit is higher as the inclination of the plate decreases to obtain enough intersections. Eventually, if the plate is normal to $\mathbf{k}_{\mathrm{r}}$, the formula for the specular reflection case in (15) should be used.
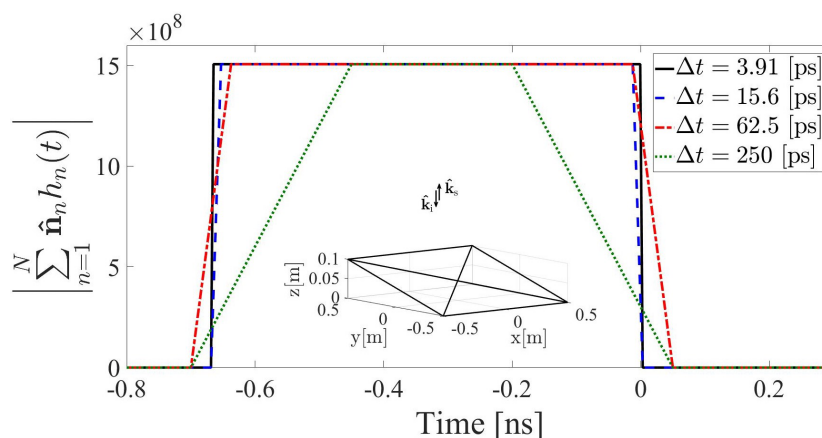
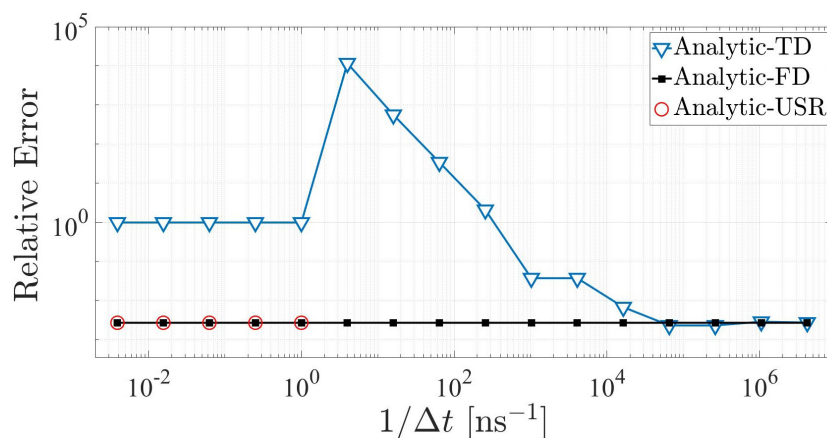**Figure 4**. Norm of the total PO integral of the plate.

Figure 5. Comparison of the relative error in the backscattered RCS.

4. Conclusion

The complete formulation of the closed-form evaluation of the PO integral on linear triangular patches in time domain is presented. Numerical examples show that even the closed-form expressions are used, time step size should be chosen considering the triangle sizes, incident and observation directions (or spatial steps), since for a fixed time step size, the accuracy of the solution depends on the norm of $\mathbf{k}_r$. If the scatterer fits into two consecutive time steps and the $\mathbf{k}_r$-plane does not intersect with the scatterer at all, the formula for the USR case can be used.

References

[1] Gordon WB. High frequency approximations to the physical optics scattering integral. IEEE Transactions on Antennas and Propagation 1994; 42 (3): 427-432. doi: 10.1109/8.280733

[2] Bölükbaş, D, Ergin AA. A Radon transform interpretation of the physical optics integral. Microwave and Optical Technology Letters 2005; 44 (3): 284-288. doi: 10.1002/mop.20612

[3] Ülkü HA, Ergin AA. Radon transform interpretation of the physical optics integral and application to near and far field acoustic scattering problems. IEEE Transactions on Antennas and Propagation 2010; 1-4. doi: 10.1109/APS.2010.5562314

[4] Karaca S, Ergin AA. Closed-form time domain PO expressions of the electric field scattered from PEC objects illuminated by an electric dipole. IEEE Transactions on Antennas and Propagation 2015; 63 (10): 4477-4485. doi: 10.1109/TAP.2015.2456973

[5] Zhou X, Cui TJ. A closed-form representation of time-domain far fields based on physical optics. IEEE Antennas and Wireless Propagation Letters 2012; 11: 965-968. doi: 10.1109/LAWP.2012.2213331

[6] Liu J, Guo L. Fast shadowing computation for physical optics integrals in terms of Levin method. IEEE Antennas and Wireless Propagation Letters 2017; 16: 1767-1770. doi: 10.1109/LAWP.2017.2675443

[7] Chou H. A generalized physical optic-based diffraction mechanism analysis of transient scattering from perfectly conducting surfaces. IEEE Transactions on Antennas and Propagation 2019; 67 (7): 4792-4802. doi: 10.1109/TAP.2019.2908111

[8] Serim HA, Ergin AA. Computation of the physical optics integral on NURBS surfaces using a Radon transform interpretation. IEEE Antennas and Wireless Propagation Letters 2008; 7: 70-73. doi: 10.1109/LAWP.2008.915811

[9] Aktepe A, Ülkü HA. Exact evaluation of time domain physical optics integral on quadratic triangular surfaces. IEEE Transactions on Antennas and Propagation 2020; 68 (3): 7447-7456. doi: 10.1109/TAP.2020.2998167

[10] Ülkü HA, Ergin AA. Application of analytical retarded-time potential expressions to the solution of time domain integral equations. IEEE Transactions on Antennas and Propagation 2011; 59 (11): 4123-4131. doi: 10.1109/TAP.2011.2164180

[11] Jones DS. The Theory of Generalised Functions. Cambridge, UK: Cambridge University Press 1982.

[12] Lathi BP. Linear Systems and Signals. Oxford, UK: Oxford University Press, 2004.

[13] Shanker B, Ergin AA, Lu MY, Michielssen E. Fast analysis of transient electromagnetic scattering phenomena using the multilevel plane wave time domain algorithm. IEEE Transactions on Antennas and Propagation 2003; 51 (3): 628-641. doi: 10.1109/TAP.2003.809054

[14] Liu Y, Al-Jarro A, Bagci H, Michielssen E. Parallel PWTD accelerated explicit solution of the time-domain electric field volume integral equation. IEEE Transactions on Antennas and Propagation 2016; 64 (6): 2378-2388. doi: 10.1109/TAP.2016.2546964

[15] Jenn D. Radar and Laser Cross Section Engineering. Reston, VA, USA: AIAA, 1995.

[16] Balanis CA. Advanced Engineering Electromagnetics. Hoboken, NJ, USA: John Wiley & Sons, 1989.